REPORT DOCUMENTATION PAGE

Form Approved
OMB No. 0704-0188

The public reporting burden for this collection of information is estimated to average 1 hour per response, including the time for reviewing instructions, searching existing data sources, gathering and maintaining the data needed, and completing and reviewing the collection of information. Send comments regarding this burden estimate or any other aspect of this collection of information, including suggestions for reducing the burden, to Department of Defense, Washington Headquarters Services, Directorate for Information Operations and Reports (0704-0188), 1215 Jefferson Davis Highway, Suite 1204, Arlington, VA 22202-4302. Respondents should be aware that notwithstanding any other provision of law, no person shall be subject to any penalty for failing to comply with a collection of information if it does not display a currently valid OMB control number.

PLEASE DO NOT RETURN YOUR FORM TO THE ABOVE ADDRESS.

1. REPORT DATE *(DD-MM-YYYY)*	2. REPORT TYPE	3. DATES COVERED *(From - To)*
	Technical Report - reprint	June 2005 - April 2009

4. TITLE AND SUBTITLE

Nested Markov chain Monte Carlo sampling of a density functional theory potential: Equilibrium thermodynamics of dense fluid nitrogen

5a. CONTRACT NUMBER

W911NF-05-1-0265

5b. GRANT NUMBER

5c. PROGRAM ELEMENT NUMBER

6. AUTHOR(S)

Joshua D. Coe, Thomas D. Sewell, and M. Sam Shaw

5d. PROJECT NUMBER

W911NF-05-1-0265

5e. TASK NUMBER

5f. WORK UNIT NUMBER

7. PERFORMING ORGANIZATION NAME(S) AND ADDRESS(ES)

Thompson & Sewell Research Groups, Department of Chemistry
University of Missouri-Columbia
Columbia, MO 65211

8. PERFORMING ORGANIZATION REPORT NUMBER

9. SPONSORING/MONITORING AGENCY NAME(S) AND ADDRESS(ES)

U. S. Army Research Office
P.O. Box 12211
Research Triangle Park, NC 27709-2211

10. SPONSOR/MONITOR'S ACRONYM(S)

11. SPONSOR/MONITOR'S REPORT NUMBER(S)

48101-EG-MUR

12. DISTRIBUTION/AVAILABILITY STATEMENT

Approved for public release; federal purpose rights

13. SUPPLEMENTARY NOTES

14. ABSTRACT

An optimized variant of the nested Markov chain Monte Carlo [n(MC)2] method [JChem. Phys. 130, 164104(2009) is applied to fluid N2. In this implementation of n(MC)2, isothermal-isobaric (NPT) ensemble sampling on the basis of a pair potential (the "reference" system) is used to enhance the efficiency of sampling based on Perdew–Burke–Ernzerhof density functional theory with a 6-31G* basis set (PBE/6-31G*, the "full" system). A long sequence of Monte Carlo steps taken in the reference system is converted into a trial step taken in the full system; for a good choice of reference potential, these trial steps have a high probability of acceptance. Using decorrelated samples drawn from the reference distribution, the pressure and temperature of the full system are varied such that its distribution overlaps maximally with that of the reference system. Optimized pressures and temperatures then serve as input parameters for n(MC)2 sampling of dense fluid N2 over a wide range of thermodynamic conditions. The simulation results are combined to construct the Hugoniot of nitrogen fluid, yielding predictions in excellent agreement with experiment.

15. SUBJECT TERMS

Detonation products, Equation of state, Hugoniot, Monte Carlo, Condensed phase electronic structure theory

16. SECURITY CLASSIFICATION OF:			17. LIMITATION OF ABSTRACT	18. NUMBER OF PAGES	19a. NAME OF RESPONSIBLE PERSON
a. REPORT	b. ABSTRACT	c. THIS PAGE			Dr. Donald L. Thompson, PI
U	U	U	U	11	19b. TELEPHONE NUMBER *(Include area code)* 573-882-0051

Reset

Standard Form 298 (Rev. 8/98)
Prescribed by ANSI Std. Z39.18

Nested Markov chain Monte Carlo sampling of a density functional theory potential: Equilibrium thermodynamics of dense fluid nitrogen

Joshua D. Coe,[1,a)] Thomas D. Sewell,[2] and M. Sam Shaw[1]
[1]*Theoretical Division, Los Alamos National Laboratory, Los Alamos, New Mexico 87545, USA*
[2]*Department of Chemistry, University of Missouri-Columbia, Columbia, Missouri 65211-7600, USA*

(Received 17 April 2009; accepted 20 July 2009; published online 17 August 2009)

An optimized variant of the nested Markov chain Monte Carlo [n(MC)^2] method [J. Chem. Phys. **130**, 164104 (2009)] is applied to fluid N_2. In this implementation of n(MC)^2, isothermal-isobaric (*NPT*) ensemble sampling on the basis of a pair potential (the "reference" system) is used to enhance the efficiency of sampling based on Perdew–Burke–Ernzerhof density functional theory with a 6-31G* basis set (PBE/6-31G*, the "full" system). A long sequence of Monte Carlo steps taken in the reference system is converted into a trial step taken in the full system; for a good choice of reference potential, these trial steps have a high probability of acceptance. Using decorrelated samples drawn from the reference distribution, the pressure and temperature of the full system are varied such that its distribution overlaps maximally with that of the reference system. Optimized pressures and temperatures then serve as input parameters for n(MC)^2 sampling of dense fluid N_2 over a wide range of thermodynamic conditions. The simulation results are combined to construct the Hugoniot of nitrogen fluid, yielding predictions in excellent agreement with experiment. © *2009 American Institute of Physics*. [DOI: 10.1063/1.3200904]

I. INTRODUCTION

The behavior of matter subjected to extreme conditions is a topic of abiding interest, having direct application to shock physics[1] as well as the planetary[2] and geosciences.[3] Its relevance to the latter has assumed new importance in the wake of global climate change, as sequestration of CO_2 in underground reservoirs may constitute a vital component in emission-free processing of fossil fuels.[4] The focus here will be on equilibrium characterization of warm, dense fluids such as those produced by detonation of high explosive (HE) compounds. Specifically, Monte Carlo (MC) simulation[5,6] will be used to characterize the locus of accessible shock states (known as the Hugoniot locus[7]) for molecular nitrogen fluid, an almost ubiquitous component of HE detonation product mixtures.

Recently[8] (hereafter, we will refer to Ref. 8 as Paper 1) we reported a thermodynamic optimization procedure designed to improve the sampling efficiency of the nested Markov chain Monte Carlo [n(MC)^2] method.[9,10] The n(MC)^2 procedure partitions a standard MC simulation into a reference system defined by an approximate potential and a full system defined by an alternative, more accurate one. A sequence of elementary moves (in the *NPT* ensemble, these correspond to single-particle displacements or volume adjustments), each accepted with Boltzmann weight in the reference system, is used to build a many-particle composite trial step taken in the full system. A slight modification of the acceptance criterion for these extended trial steps recovers Metropolis sampling of the full potential without having to evaluate it at each configuration. The approach developed in Paper 1 improved the efficiency of the n(MC)^2 technique by allowing the thermodynamic states of the reference and full systems to vary independently such that their respective distributions attained maximal overlap, thereby raising the mean acceptance probability for trial composite steps. Because the purpose of Paper 1 was merely to illustrate the procedure, the reference and full systems were defined by model potentials not differing in computational expense. The present work serves both to extend the application of optimized (*o*-) n(MC)^2 to a full system characterized by density functional theory (DFT) (Ref. 11) and to construct the shock Hugoniot locus of fluid N_2 at this level of theory.

The following section describes in detail the potentials used, an analytical pair potential for the reference system and DFT for the full system. Section III reviews the principal expressions making up the *o*-n(MC)^2 procedure, referring the reader to previous works for their full justification. Section IV outlines the continuum theory of shock waves as expressed in the Rankine–Hugoniot relations as well as the implementation of these relations in the context of atomistic simulation; this linkage is then illustrated by construction of the N_2 Hugoniot locus from the *o*-n(MC)^2 simulation results discussed in Sec. III. The final section summarizes and offers some thoughts on future implementation of the procedure.

II. POTENTIAL ENERGY EVALUATION

A. Specification of the full potential

DFT replaces the antisymmetric *N*-electron wavefunction, expressed in spin-spatial coordinates $\mathbf{x}$,

$$\Psi \equiv \Psi(\mathbf{x}_1,\mathbf{x}_2,\ldots,\mathbf{x}_N), \tag{1}$$

with the spatial density of a single electron,

a)Electronic mail: jcoe@lanl.gov.

 © 2009 American Institute of Physics

Downloaded 05 Apr 2010 to 128.206.89.92. Redistribution subject to AIP license or copyright; see http://jcp.aip.org/jcp/copyright.jsp

$$\rho(\mathbf{r}) = N \int \cdots \int |\Psi(\mathbf{x}_1, \mathbf{x}_2, \ldots, \mathbf{x}_N)|^2 ds_1 d\mathbf{x}_2 \cdots d\mathbf{x}_N. \quad (2)$$

Although this procedure appears to entail considerable information loss, the first Hohenberg–Kohn theorem[12] guarantees a unique map from the density to the ground state energy, E_g,

$$\rho \Rightarrow \hat{H} \Rightarrow \Psi \Rightarrow E_g. \quad (3)$$

E_g can then be expressed as a functional of the density, $E_g[\rho]$, and its constituent parts decomposed[13] in the following manner:

$$E_g[\rho] = T_S[\rho] + J[\rho] + E_{\mathrm{Ne}}[\rho] + E_{\mathrm{XC}}[\rho]. \quad (4)$$

The various contributions to the total electronic energy are, respectively, the kinetic energy for a gas of noninteracting electrons, the (mean-field) Coulombic repulsion, the Coulombic electron-nuclear attraction, and the exchange-correlation functional. The first three terms are analytically soluble whereas the fourth subsumes all quantum effects (including real-time, dynamic electron correlation, the Pauli principle, the self-interaction correction,[14] and correlated electron contributions to the kinetic energy) and has so far proven strongly resistant to universal description. Although exchange-correlation functionals constructed entirely from first principles have been reported,[15] most $E_{\mathrm{XC}}[\rho]$ are built from fits to a set of experimental and/or *ab initio* data. Different functionals, then, are distinguished primarily by their exchange-correlation component, $E_{\mathrm{XC}}[\rho]$. The second Hohenberg–Kohn theorem[12] establishes a variational principle for the density in the same manner as for the wavefunction, and the Kohn–Sham equations[13] permit iterative solution for a set of one-electron orbitals in the same manner as the Roothaan equations[16] in Hartree–Fock.

All of the quantum chemical calculations reported below were carried out using GAUSSIAN03.[17] In test calculations on a periodic cubic cell containing 100 N_2 at density $\rho = 1.46\ \mathrm{g/cm^3}$, we evaluated the performance of four different $E_{\mathrm{XC}}[\rho]$: BLYP,[18,19] PBE,[20] PW91,[21] and BVWN.[18,22] All periodic calculations of the liquid-state energy were performed at the Γ-point.[23] In addition to the relative computational speed at the point of basis set convergence, we compared the computed bond length and frequency of the isolated molecule to their experimental values.

The basis sets examined cover the range from minimal [STO-3G (Ref. 24)] to triple zeta with polarization (*d* and *f*) functions, the latter containing 70 basis functions for each molecule. There is no evidence of ionization at the densities of interest here, so diffuse functions were neither necessary nor desirable; energies computed using the 6-311G(3*df*,3*pd*) basis[25] were thus treated as the complete basis set limit (CBSL) for each functional. Table I records the percent deviation in the total energy (relative to that of 100 isolated N_2 molecules) for a periodic box of 100 N_2 molecules in a typical liquid-state configuration drawn from the reference distribution, calculated as a function of $E_{\mathrm{XC}}[\rho]$ and basis set, from that calculated with the same functional at the CBSL. All energies were corrected for basis set superposition error (BSSE),[26] the spurious stabilization conferred upon an atomic center by basis functions "borrowed" from another atom. Our target accuracy for the nitrogen Hugoniot was ~1%, and although this value does not translate directly to an accuracy constraint on the DFT energy, it does serve as a useful guide. All four functionals tested were converged to roughly 1% at the 6-31G* (Refs. 27 and 28) level, although the performance of PW91 is noticeably worse than that of the other three. Because full system energies computed using any of the four functionals paired with 6-31G* yielded good accuracy in reasonable time, this basis set was singled out for further tests on the isolated molecule.

TABLE I. Percent deviation of the BSSE-corrected energy of 100 N_2 molecules at density of $\rho = 1.46\ \mathrm{g/cm^3}$, as a function of basis set and $E_{\mathrm{XC}}[\rho]$, from that calculated using the same functional at the CBSL [defined as 6-311G(3*df*,3*pd*) (Ref. 25)]. Three of the four functionals tested are converged to roughly 1% using the 6-31G* basis. Based on these results, the 6-31G* basis set was used in all subsequent calculations reported in this study.

Basis set	BLYP[a]	PW91[a]	PBE[a]	BVWN[a]
STO-3G[a]	−40.2	−42.9	−33.8	−34.1
6-31G[b]	2.5	4.6	5.3	0.8
6-31G*[a]	−1.1	−3.1	−1.4	−1.4
6-311G**[c]	−1.0	−2.0	−1.1	−0.7

[a]See text for reference.
[b]Reference 52.
[c]References 27 and 53

Ground state properties recorded in Table II reflect little variation among the various flavors of DFT, although it is interesting that all four outperformed MP2 (Ref. 29) in predicting *l*, the equilibrium bond length (correcting for anharmonicity makes the MP2 value even worse relative to those of DFT). The rightmost column of Table II compares relative timings for each functional paired with the 6-31G* basis set, and speedup factors were defined as the ratio of time τ needed to compute the energy of the full box of 100 N_2 to a reference value τ_{ref},

$$\text{speedup} = \frac{\tau}{\tau_{\mathrm{ref}}}. \quad (5)$$

The reference time was defined to be that required by the slowest functional, giving it a speedup factor of unity. PW91

TABLE II. Performance of several exchange-correlation functionals in comparison to those of MP2 and experiment. Points of comparison include ground state bond length *l* and (harmonic-approximation) frequency ω of the isolated N_2 molecule, as well as the relative time required for a three-dimensional periodic single-point calculation on the fluid sample of 100 N_2 molecules. All calculations used the 6-31G* basis set. Speedup factors are defined in the text, the largest value corresponding to the fastest time and the slowest assigned a factor of unity. Based on the results of this simulation, the PBE functional was chosen for use in all subsequent calculations reported.

EXC	*l* (Å)	ω ($\mathrm{cm^{-1}}$)	Speedup
BLYP	1.118	2337	1.00
PBE	1.117	2360	1.13
PW91	1.116	2364	1.14
BVWN	1.116	2346	1.09
MP2	1.131	2175	…
Expt[a]	1.094	2359	…

[a]Reference 39.

Downloaded 05 Apr 2010 to 128.206.89.92. Redistribution subject to AIP license or copyright; see http://jcp.aip.org/jcp/copyright.jsp

was fastest, although the difference with PBE was practically negligible. On the basis of its being well converged at the 6-31G* level, predicting satisfactory ground state properties, and (almost) recording the fastest calculation time, the PBE functional was chosen for all subsequent calculations.

We conclude this section with a note regarding omission of local density approximation (LDA) functionals. Although not shown, we also tested SLYP[19,30] and SVWN[22,30] in addition to the generalized gradient approximation functionals examined above. Calculated energies dropped steadily on approach to the CBSL, actually dipping well below zero in the case of SLYP. A negative energy would imply that it is thermodynamically preferable for a sample of nitrogen gas to compress spontaneously to a density of 1.46 g/cm^3, clearly indicating catastrophic failure of LDA in describing the dense N_2 fluid sample.

B. Parametrization of the reference potential

Vital to our scheme for building equilibrium averages with DFT energies was a rapidly computable potential function capturing enough of the essential physics to serve as an adequate reference for the DFT. After having converged an accurate combination of exchange-correlation functional and basis set, we parametrized the reference potential on the basis of this model chemistry.

The exponential-6 (Buckingham) potential was used to describe pairwise interaction, φ_{ab}, of atomic sites a and b. The sites reside on diatomic molecules i and j, so the complete interaction for a pair of reference system molecules is summarized in

$$\varphi(r_{ab}) = \frac{\varepsilon}{\alpha - 6}\left(6e^{\alpha(1-r_{ab})} - \frac{\alpha}{r_{ab}^6}\right) \tag{6}$$

and

$$\varphi_{ij} = \sum_{a=1}^{2}\sum_{b=1}^{2}\varphi(r_{ab}). \tag{7}$$

The site-site radii can be re-expressed in terms of the center-of-mass (c.m.) separation vector $\mathbf{r}_{ij}$ and bond vectors $\mathbf{l}_i$ and $\mathbf{l}_j$ (of lengths l_i and l_j),

$$r_{ab}^2 = \frac{0.25r_{ij}^2(l_i^2 + l_j^2) + (-1)^a(\mathbf{r}_{ij}\cdot\mathbf{l}_i) + (-1)^b(\mathbf{r}_{ij}\cdot\mathbf{l}_j) + (-1)^{a+b}0.5(\mathbf{l}_i\cdot\mathbf{l}_j)}{r_0^2}. \tag{8}$$

Bond lengths were fixed at $l=1.117$ Å, the value predicted by PBE/6-31G* for the isolated N_2 molecule. Parameters ε, α, and r_0 represent the depth of the well, the steepness of the repulsive wall, and the position of the minimum, respectively; their fitted values and the process used to obtain them are provided below. Although Eq. (6) realistically captures the exponential character of hard-core repulsion and the r^{-6} dependence of dispersion at long range,[31] it also diverges to $-\infty$ at very short range. Using the parameter set described below, the potential function defined by Eqs. (6)–(8) reaches a maximum value of 9×10^4 K at $r_{ab}\approx1.15$ Å, so enforcing a minimum allowable separation $r_{\min}=1.20$ Å safely avoided the (unphysical) strongly attractive forces present at small values of r_{ab}.

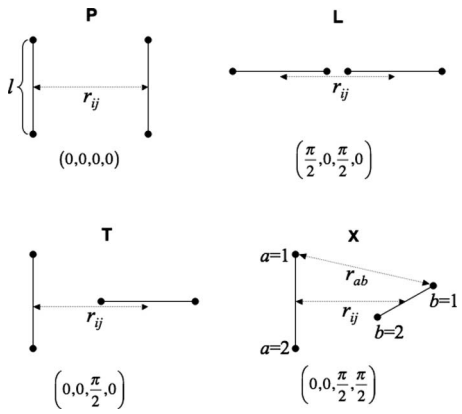

FIG. 1. Diatomic pair configurations used to parametrize the reference potential whose behavior is illustrated in Fig. 2. Bond lengths were held fixed at $l=1.117$ Å, while c.m. separations r_{ij} were swept over a range of roughly 1.6–6.6 Å, depending on the configuration type (see text). Configuration types are characterized by four angles, $(\theta_1,\chi_1,\theta_2,\chi_2)$, where θ and χ represent rotation of molecules 1 and 2 within and out of the plane of the page. Clockwise rotations are positive, and all angle values are zeroed to those of the P configuration.

In order to ensure suitable parameter values, Eq. (6) was fitted to a set of PBE/6-31G* energies for the N_2 dimer relative to those for a pair of isolated N_2 molecules. The distribution of pair configurations sampled in a fluid was approximated using the four fiducial configuration types depicted in Fig. 1, denoted as P, L, T, and X. Center-of-mass distances were scanned over ranges of 1.59–4.23 Å (X), 1.85–4.50 Å (P), 1.59–5.29 Å (T) and 2.38–6.62 Å (L) in roughly 0.25 Å intervals and the difference between Eq. (6) and the PBE result was recorded. The weighted sum of these differences, squared, was then minimized over the domain of the parameter set,

$$\min_{\alpha,\varepsilon,r_0}\ \mathrm{Err} = \min_{\alpha,\varepsilon,r_0}\left\{\sum_{l=1}^{4}\sum_{k=1}^{N_l} w_{k,l}(\varphi_{ij}^{\mathrm{DFT}}(k,l) - \varphi_{ij}^{\text{exp-6}}(k,l))^2\right\}, \tag{9}$$

where l runs over the set of pair configuration types $\{P,L,T,X\}$ and k indexes the N_l discrete values of r_{ij}. The weights,

Downloaded 05 Apr 2010 to 128.206.89.92. Redistribution subject to AIP license or copyright; see http://jcp.aip.org/jcp/copyright.jsp

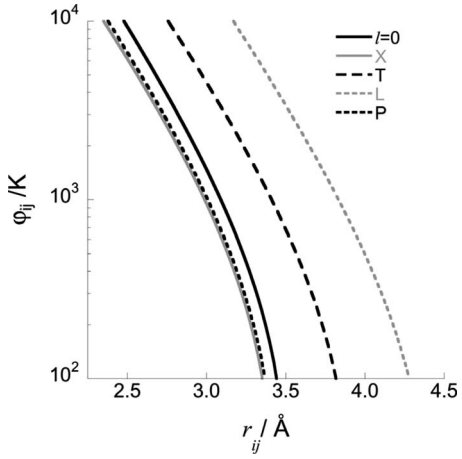

FIG. 2. The pair potential defined by Eqs. (6)–(8) and (12) as a function of c.m. separation r_{ij} for the diatomic pair configurations illustrated in Fig. 1 (X, T, L, and P) and a fixed bond length $l=1.117$ Å. Comparison of these curves with the purely spherical potential ($l=0$ Å) reveals the anisotropic character of φ_{ij}. Note that the ordinate is plotted on a log scale.

$$w_{k,l} = \frac{1}{(\max\{\varphi_{ij}^{\mathrm{DFT}}(k,l), \varphi_{\mathrm{sw}}\})^2}, \tag{10}$$

were chosen to forestall disproportionate contributions from large c.m. separations (unlikely to be of much importance in the dense fluid regime sampled below) by setting $\varphi_{\mathrm{sw}} = 1000$ K, and the weighted root mean square error (wRMSE) was evaluated as

$$\mathrm{wRMSE} = \sqrt{\frac{\mathrm{Err}}{\Sigma_{l=1}^{4} N_l}}. \tag{11}$$

This procedure yielded the following best-fit parameter values

$$\varepsilon = 34.156 \text{ K}, \quad r_0 = 4.037 \text{ Å}, \quad \alpha = 12.29, \tag{12}$$

with a wRMSE of 0.189. At fixed parameter values φ_{ab} is determined entirely by the site-site separation (r_{ab}), but it is important to note that the full interaction of two diatomics (φ_{ij}) is highly anisotropic. The character of the reference potential defined by Eqs. (6)–(8) and (12) is illustrated in Fig. 2, where we have plotted φ_{ij} over a range of r_{ij} for the four fiducial configuration types shown in Fig. 1. These should be compared not only with one another but also with a purely spherical potential ($l=0$) for which the four configuration types collapse into one.

In order to estimate the magnitude of many-body effects, we compared the standard pair energy,

$$U_{AB}^{(2)} = U_{AB} - U_A - U_B, \tag{13}$$

with an "effective" pair energy for molecules in the liquid,

$$U_{AB}^{*} = U_{\mathrm{box}} + U_{\mathrm{box}\text{-}AB} - U_{\mathrm{box}\text{-}A} - U_{\mathrm{box}\text{-}B}, \tag{14}$$

where U_A (U_B) is the total energy of isolated molecule $A(B)$, U_{AB} is that of two molecules taken together, U_{box} is the energy of a box containing 100 molecules in the liquid state, and $U_{\mathrm{box}\text{-}X}$ is that of the same box with the designated molecule or pair removed. Under the assumption that many-body effects terminate at three-body interactions, it can be shown (see Appendix A) that the sum over all A and B of $U_{AB}^{*} - U_{AB}^{(2)}$ gives the many-body energy of the sample to within a constant factor. For a pair of molecules[32] taken from a liquid-state configuration at $T=3267$ K and $P=16.8$ GPa, $U_{AB}^{(2)}/k_B = 4519$ K and $U_{AB}^{*}/k_B = 3030$ K [it is important to note that in evaluating Eqs. (13) and (14), all atoms removed were replaced with a ghost basis set just as in standard counterpoise calculations], giving a many-body stabilization per pair of approximately 1500 K, or one-third of the isolated pair energy. Although a rough estimate only, this provides strong *prima facie* evidence of an appreciable many-body contribution to the energy, and thus motivation for moving beyond straightforward use of pair potentials when high accuracy is required.

III. NESTED MARKOV CHAIN MONTE CARLO SAMPLING

The following provides only a brief overview of o-n(MC)^2; for a more complete treatment, see Paper 1. In standard MC sampling with the Metropolis algorithm, a trial step drawn from a uniform distribution (also known as the marginal distribution) is accepted with probability[33]

$$\alpha_{ij} = \min\left(\frac{\pi_j}{\pi_i}, 1\right), \tag{15}$$

where π_k represents the relative weight assigned to configuration space point k. $\pi_k \propto e^{W_k}$ in classical statistics and W_k is a thermodynamic function appropriate to the ensemble being sampled. In the isothermal–isobaric (NPT) ensemble used below, W is defined as

$$W_k \equiv -\beta(U_k + PV_k) + N \ln V_k, \tag{16}$$

the final term of which results from the use of scaled coordinates.[5,34] U, V, and β represent internal energy, volume, and inverse temperature $(kT)^{-1}$, respectively. Trial moves consist of single-particle displacements and volume adjustments, and the relative probabilities of attempted move types are chosen *a priori* according to the needs of the simulation. Ensemble averages of some property X can be approximated by discrete quadrature according to

$$\langle X \rangle_{NPT} = \frac{\int \pi(\tau,V) X d\tau dV}{\int \pi(\tau,V) d\tau dV} \approx \frac{1}{N_s} \sum_{i=1}^{N_s} X_i, \tag{17}$$

where τ represents the full array of system coordinates and the sum runs over the N_s configurations sampled by the MC simulation. The variance in such averages will decrease as N_s rises and, in the limit of fully decorrelated samples, the scaling relation assumes the well-known form $\sigma_X \sim N_s^{-1/2}$. Configurations sampled consecutively using standard MC are related by elementary moves; that is, they are *highly* correlated. If the system energy is expressible in a simple analytical form, then the use of highly correlated samples can be compensated for by accumulating sufficiently large values of N_s. The difficulty arises when one requires both

Downloaded 05 Apr 2010 to 128.206.89.92. Redistribution subject to AIP license or copyright; see http://jcp.aip.org/jcp/copyright.jsp

high accuracy, such as that offered by an *ab initio* or DFT potential, and high precision, which requires many decorrelated sampling points. If each acceptance test (energy evaluation) is costly in terms of computing time, then being forced to collect strongly correlated samples may preclude precision sampling on purely practical grounds.

A method for sampling an accurate and expensive potential without requiring the strongly correlated samples of conventional MC was introduced by Iftimie *et al.*,[9] reformulated by Gelb,[10] and refined by the current authors.[8] The n(MC)^2 method concatenates a sequence of elementary moves, each accepted with Boltzmann weight on the basis on an approximate reference potential. At the endpoints of this sequence a modified Metropolis test is used to recover a Boltzmann distribution of states based on a different (and hopefully, more accurate) potential. We will refer to the elementary steps taken independently as *reference* steps (taken in the reference *system*), and the entire sequence of reference steps bookended by evaluations of the second potential as a *full* step (taken in the full system, characterized by the full potential.) Consecutive full system energies are partially decorrelated by the intervening sequence of reference steps. If the full potential is more expensive than the reference potential, then n(MC)^2 lowers the total cost of the calculation by limiting the N_s required for a target σ_X on averages taken in the full system. Indicating reference system quantities with superscripted "0," the form of the acceptance probability required for Metropolis sampling of the partially decorrelated (full) potential is[8–10]

$$\alpha_{ij} = \min\left(1, \frac{\pi_j}{\pi_i}\frac{\pi_i^{(0)}}{\pi_j^{(0)}}\right). \tag{18}$$

To summarize, *a sequence of trial steps taken in the reference system and accepted according to* (15) *is used to build a trial step taken in the full system that is accepted according to* (18). Note that the standard ratio of Boltzmann factors for the initial and final states in the full system has been "corrected" by the inverse of this ratio for the reference system. Following our previous treatment, we express the difference in full and reference system weights for state k as $\delta W_k \equiv W_k - W_k^{(0)}$ and the difference in δW for consecutive full system configurations as $\Delta W \equiv \delta W_i - \delta W_j$. Equation (18) can then be recast as

$$\alpha_{ij} = \begin{cases} 1, & \Delta W \geqslant 0 \\ e^{\Delta W}, & \Delta W < 0. \end{cases} \tag{19}$$

The total speedup factor S gained by sampling the full potential with n(MC)^2 rather than with traditional MC can be given in terms of the computing time needed to reach a target variance requiring N_d decorrelated evaluations of the full potential. The cost of collecting these directly through standard Metropolis sampling is

$$\Lambda = N_d O_{\mathrm{corr}} \lambda, \tag{20}$$

where λ is the computational expense of making an elementary move with the full potential. O_{corr} is an effective correlation length (assumed to be roughly equal for reference and full potentials) statistically equivalent to a single random sample drawn from the distribution. It is only an effective length in the sense that it incorporates the inefficiency of rejected steps as well as net motion through configuration space, and therefore it will vary with the maximum trial step radius. For the purposes of this discussion, we assume this radius to be set such that the mean acceptance probability of elementary trial steps made using either potential is the same. The total cost of collecting N_d decorrelated samples using the n(MC)^2 procedure is then

$$\Lambda' = \frac{N_d O_{\mathrm{corr}} \lambda^{(0)} + \dfrac{N_d O_{\mathrm{corr}} \lambda}{O}}{\overline{\alpha}}, \tag{21}$$

where $\lambda^{(0)}$ is the cost of an elementary move made with the reference potential, $\overline{\alpha}$ is the mean acceptance probability of trial composite steps, and O is the number of reference steps comprising a single composite step. The speedup factor is the ratio of Λ and Λ',

$$S = \frac{\Lambda}{\Lambda'} = \frac{\overline{\alpha}\lambda}{\lambda^{(0)} + \dfrac{\lambda}{O}}. \tag{22}$$

In his presentation of n(MC)^2, Gelb[10] made the additional simplification that $\lambda/\lambda^{(0)} = O(N)$ when a pair potential is used as reference for an N-body potential such as DFT. Because the prefactor in such scaling relations can be highly significant, we include it explicitly and simplify Eq. (22) further such that

$$S = \frac{\overline{\alpha}}{\dfrac{1}{\kappa N} + \dfrac{1}{O}}, \tag{23}$$

where $\lambda/\lambda^{(0)} = \kappa N$. Although we have not attempted to quantify κ carefully, a conservative estimate of its value in our simulations is $O(10^7)$, whereas a large value for O would be $O(10^3)$. Therefore we ignore the first term in the denominator and obtain as an approximate speedup factor

$$S \approx \overline{\alpha} O. \tag{24}$$

This is an intuitively satisfying result, indicating that when the cost of evaluating the reference potential is negligible compared to that of evaluating the full potential, the speedup from using n(MC)^2 over MC is roughly equal to the effective length (actual length tempered by average probability of acceptance) of composite steps taken in the full system.

The presence of $\overline{\alpha}$ in the denominator of Eq. (21) suggests a simple prescription for raising the value of S: Increase the mean acceptance probability of trial composite steps. Although composite steps built from a sequence of elementary steps taken on the reference potential lower the correlation between consecutive evaluations of the full potential, differences between the reference and full system distributions impose practical limits on the length of these sequences. That is, because the distributions generally will peak in different regions of configuration space, the greater the number of elementary steps taken on the reference potential between acceptance tests taken on the full potential,

Downloaded 05 Apr 2010 to 128.206.89.92. Redistribution subject to AIP license or copyright; see http://jcp.aip.org/jcp/copyright.jsp

the more the reference system Markov chain will "drift" back to the center of its own distribution (see especially Figs. 11–14 in Paper 1) and thereby lower the mean acceptance probability of trial composite steps. Conversely, the greater the difference in distribution of reference and full potentials, the lower the mean acceptance probability of trial composite steps built from a fixed number of elementary steps taken on the reference potential. It would seem, then, that raising the mean acceptance probability of trial composite steps requires shifting one or both of the reference and full distributions such that their overlap is enhanced.

As detailed in Paper 1, the average acceptance probability for n(MC)^2 steps can be expressed exactly in the limit that a pair of configurations i and j are decorrelated. We express the mean acceptance probability in this limit as

$$\overline{A} \equiv \lim_{O \to O_{\mathrm{corr}}} \overline{\alpha}. \tag{25}$$

An initial state i will, by construction, possess relative weight e^{W_i} if the goal is to sample the full distribution. The final state j will, in the O_{corr} limit, be drawn randomly from the reference distribution and thus carry weight $e^{W_i^{(0)}}$. Note that the acceptance probability α_{ij} given in Eq. (18) also can be expressed in terms of δW and $W^{(0)}$ for states i and j so that α_{ij} averaged over the configuration and volume spaces of all decorrelated (i,j) pairs gives

$$\begin{aligned}\overline{A} &= \frac{\int\int\int\int \alpha_{ij} e^{W_i + W_j^{(0)}} d\tau_i dV_i d\tau_j dV_j}{\int\int\int\int e^{W_i + W_j^{(0)}} d\tau_i dV_i d\tau_j dV_j} \\ &= \frac{\int\int\int\int \alpha_{ij} e^{\delta W_i} (e^{W_i^{(0)} + W_j^{(0)}}) d\tau_i dV_i d\tau_j dV_j}{\int\int\int\int e^{\delta W_i} (e^{W_i^{(0)} + W_j^{(0)}}) d\tau_i dV_i d\tau_j dV_j}.\end{aligned} \tag{26}$$

The integrals in Eq. (26) can be estimated by sampling δW at N_{rw} configurations drawn from the reference distribution; for the combination of potentials used here, $N_{\mathrm{rw}} = O(100)$. We refer to this process as the reweighting[35] calculation, and estimates of $\overline{A}$ built in this manner will be denoted $\overline{A}_{\mathrm{rw}}$. Note that the terms appearing in parenthesis in Eq. (26) are present implicitly when i and j are sampled from the reference distribution so that Eq. (26) can be written more succinctly as

$$\overline{A} = \frac{\langle\langle \alpha_{ij} e^{\delta W} \rangle\rangle_0}{\langle\langle e^{\delta W} \rangle\rangle_0}, \tag{27}$$

where the subscripted zeros indicate that the distribution being sampled is that of the reference potential. Because the δW appearing in Eq. (26) depend on the full system pressure and temperature through Eq. (16), a single set of N_{rw} points sampled from the reference distribution at a given $P^{(0)}$ and $T^{(0)}$ can be used to build a family of $\overline{A}_{\mathrm{rw}}$ varying parametrically as functions of P and T. It is appropriate to express $\overline{A}_{\mathrm{rw}}$ as a function of all four thermodynamic variables, $\overline{A}_{\mathrm{rw}} \equiv f(P^{(0)}, T^{(0)}, P, T)$, and all subsequent references to $\overline{A}_{\mathrm{rw}}$ will list them in this order. Note that $\overline{A}_{\mathrm{rw}}$ is an *a priori* estimate of acceptance probability for composite steps taken with the n(MC)^2 procedure in that it predicts acceptance probabilities without reliance upon an actual n(MC)^2 simulation. If one desires full system thermodynamic data at $(P = P', T = T')$, a reweighting calculation performed at those conditions can be followed by variation in P and T so as to maximize $\overline{A}_{\mathrm{rw}}$. We express this optimization procedure as follows:

$$\begin{aligned}\overline{A}_{\mathrm{rw}}^{(\max)} &\equiv \overline{A}_{\mathrm{rw}}(P', T', P_{\mathrm{opt}}, T_{\mathrm{opt}}) \\ &= \max\{\overline{A}_{\mathrm{rw}}(P^{(0)}, T^{(0)}, x, y) : P^{(0)} = P', T^{(0)} = T' : P_1 \\ &\leqslant x \leqslant P_2, T_1 \leqslant y \leqslant T_2\}.\end{aligned} \tag{28}$$

The initial domain covered by the full system variables can be chosen generously, then squeezed incrementally in conjunction with finer meshes; we have found the $\overline{A}_{\mathrm{rw}}$ surface to vary smoothly with $(x,y) = (P,T)$, as illustrated in Fig. 6 of Paper 1. There we obtained $(P = P_{\mathrm{opt}}, T = T_{\mathrm{opt}})$ for full system variables, then extrapolated linearly back to the original $(P = P', T = T')$, and applied the same transformation to the reference system variables to yield $(P^{(0)} \approx P_{\mathrm{opt}}^{(0)}, T^{(0)} \approx T_{\mathrm{opt}}^{(0)})$. In this way, optimized n(MC)^2 simulations could be carried out at the full system conditions desired but with reference system conditions designed to maximize the *a priori* acceptance probability of composite steps taken in the full system. The approach taken here is slightly different in that we performed n(MC)^2 sampling with the optimal set $(P^{(0)} = P', T^{(0)} = T', P = P_{\mathrm{opt}}, T = T_{\mathrm{opt}})$ resulting from Eq. (28). This generated full system thermodynamic conditions different from the original (P', T'), and an expansion procedure described in the next section was used to recover results at (P,T) on the Hugoniot.

Data illustrating the reweighting, optimization, and optimized n(MC)^2 simulation results are shown in Table III. The δW distribution was sampled at N_{rw} configurations drawn from the reference distribution at the $(P^{(0)} = P', T^{(0)} = T')$ pairs shown in the two leftmost columns. $\overline{A}_{\mathrm{rw}}^{(0)} \equiv \overline{A}_{\mathrm{rw}}(P', T', P', T')$ was built using Eq. (27), then maximized according to Eq. (28) to yield $\overline{A}_{\mathrm{rw}}^{(\max)}$ at $(P = P_{\mathrm{opt}}, T = T_{\mathrm{opt}})$; the resulting P_{opt} and T_{opt} are shown in the third and fourth columns of Table III. One measure of the procedure's effectiveness is the ratio of the optimized to original *a priori* acceptance probabilities, $\overline{A}_{\mathrm{rw}}^{(\max)} / \overline{A}_{\mathrm{rw}}^{(0)}$; as shown in the right side of the table, the predicted acceptance probabilities rose by factors of roughly 1.5–25. Note that minor absolute variations in $\overline{A}_{\mathrm{rw}}^{(0)}$ (a small number) can make large differences in the ratio. After maximizing $\overline{A}_{\mathrm{rw}}$ through variation in P and T as in Eq. (28), optimized n(MC)^2 simulations were performed using the $(P', T', P_{\mathrm{opt}}, T_{\mathrm{opt}})$ combinations that resulted. The number of elementary steps taken in the reference system used to build a composite step made in the full system was $O = 150$, whereas $O_{\mathrm{corr}} \approx 1000$ for the reference and full potentials chosen in Sec. II (cf. Fig. 3 in Paper 1). The average speedup factor S achieved in sampling the full potential with o-n(MC)^2 rather than traditional MC was just over 50.

No attempt was made in the present work to maximize O, the number of elementary steps in the reference system used to build a trial composite step in the full system. This potential loss of efficiency is compensated for partly by a higher mean acceptance probability at lower O values, but the ideal situation would be one in which optimization were performed directly on S rather than on $\overline{A}_{\mathrm{rw}}$. This, in turn,

Downloaded 05 Apr 2010 to 128.206.89.92. Redistribution subject to AIP license or copyright; see http://jcp.aip.org/jcp/copyright.jsp

TABLE III. Summary of the reweighting and optimization procedures described in the text. The δW distribution was sampled at N_{rw} configurations defined by the thermodynamic conditions $(P^{(0)}=P', T^{(0)}=T')$. The *a priori* acceptance probability $\bar{A}_{rw}^{(0)} \equiv \bar{A}_{rw}(P',T',P',T')$ was then calculated from Eq. (27), followed by optimization according to Eq. (28) to yield $\bar{A}_{rw}^{(max)} \equiv \bar{A}_{rw}(P',T',P_{opt},T_{opt})$. The effectiveness of the optimization is reflected in the ratio $\bar{A}_{rw}^{(max)}/\bar{A}_{rw}^{(0)}$. The speedup factor $S \approx \bar{\alpha} O$ is given for optimized n(MC)^2 simulations in which $O=150$ and $O_{corr} \approx 1000$.

$P^{(0)}=P'$	$T^{(0)}=T'$	P_{opt}	T_{opt}	N_{rw}	$\bar{A}_{rw}^{(0)}$ (%)	$\bar{A}_{rw}^{max}$ (%)	$\bar{A}_{rw}^{max}/A_{rw}^{(0)}$	S
6.30	728	4.84	615	563	0.49	4.14	8.45	41.6
9.70	1424	7.48	1200	394	0.49	8.84	18.04	55.3
11.90	1893	9.22	1606	478	0.82	3.73	4.55	60.4
14.90	2540	11.94	2206	430	0.59	6.78	11.49	55.3
15.80	2730	12.52	2355	484	0.34	7.96	23.41	52.9
19.20	3490	16.79	3267	532	2.94	9.59	3.26	64.7
20.50	3795	16.60	3270	444	0.63	13.01	20.65	53.3
20.60	3812	16.93	3417	386	2.25	8.62	3.83	56.7
23.00	4375	19.98	4079	380	1.74	7.32	4.21	27.7
23.20	4410	19.63	3886	444	2.49	5.89	2.37	76.0
23.30	4434	17.58	3361	443	1.84	3.09	1.68	34.5
23.50	4475	21.27	4308	441	3.72	5.97	1.60	55.2
24.70	4765	19.58	3854	525	0.42	1.50	3.57	60.5
25.20	4877	20.75	4362	439	2.30	3.65	1.59	56.5
27.40	5421	22.01	4769	426	0.76	3.91	5.14	60.7
28.90	5785	21.29	4765	420	1.17	3.20	2.74	40.7
30.00	6062	23.06	5156	492	0.67	2.91	4.34	41.2
40.50	8847	34.90	8308	429	5.48	7.86	1.43	40.0

would require an analytical expression for the acceptance probability in Eq. (27) in terms of O, as well as more extensive reweighting calculations over variable O. Empirical examination of the variation in $\bar{\alpha}$ with O can be found in Paper 1.

In order to limit the computational overhead of the reweighting and optimization procedures, it is desirable that $\bar{A}_{rw}^{(max)}$ converge for N_{rw} as small as possible; otherwise, efficiency gained in using the optimized form of n(MC)^2 will be lost in performing the optimization procedure itself. As discussed in Paper 1 (and particularly in connection with Figs. 7 and 8 there), $\bar{A}_{rw}^{(max)}$ tends to converge faster than (P_{opt},T_{opt}) due to its exhibiting a broad flat peak as a function of P and T. Figure 3 illustrates the convergence behavior of $\bar{A}_{rw}^{(max)}$ for five pairs of $(P=P', T=T')$ spanning the full range of conditions included in Table IV. All five states exhibited an initial decline in $\bar{A}_{rw}^{(max)}$ as reweighting samples were added but stabilized roughly in the neighborhood of $N_{rw}=100-500$. While convergence was incomplete in most cases (particularly for the more extreme thermodynamic states), it still was adequate to ensure large efficiency increases relative to standard n(MC)^2 or conventional MC sampling on the basis of the full potential.

IV. THE NITROGEN HUGONIOT

The Hugoniot locus is comprised of thermodynamic states accessible by shock loading of an initial state. In this section we describe application of the *o*-n(MC)^2 method to construction of the Hugoniot locus for N_2 fluid and compare our predictions to experimental data. Prior to doing so, however, we briefly summarize the continuum theory of shock waves as well as the statistical approximations underlying atomistic treatment.

Consider a sample of material having specific volume V_0 (volume per unit mass$=1/\rho_0$) and specific internal energy E_0, struck by a piston moving at speed u_p. If c_0 is the sound speed in the material at zero pressure and $u_p \ll c_0$, the impact will create an acoustic wave moving through the sample at speed c_0; pistons having speeds of $u_p \sim 0.01 c_0$ or greater will generate shock waves characterized by discontinuous density gradients at the wave front. Mass, momentum, and energy conservation in samples initially at rest at zero pressure

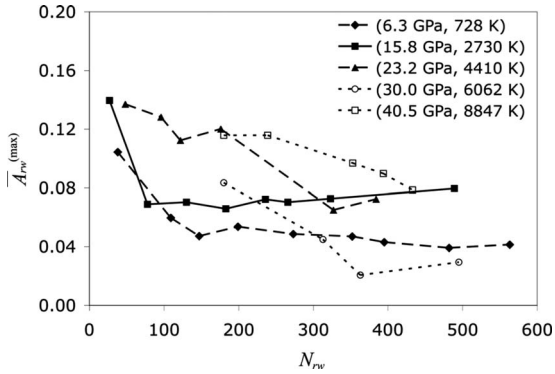

FIG. 3. Convergence behavior of $\bar{A}_{rw}$ with respect to the number of reweighted sampling points N_{rw}, for five combinations of initial $(P=P', T=T')$. All combinations show an initial decrease in acceptance probability, but level out at roughly $N_{rw}=500$. $\bar{A}_{rw}$ is an *a priori* estimate of $\bar{\alpha}$ in the decorrelated limit $(O=1000)$, and therefore much lower than the $\bar{\alpha}$ computed *a posteriori* from n(MC)^2 simulation at $O=150$.

Downloaded 05 Apr 2010 to 128.206.89.92. Redistribution subject to AIP license or copyright; see http://jcp.aip.org/jcp/copyright.jsp

TABLE IV. Summary of simulation data used in Figs. 4–8.

P (GPa)	T (K)	V (cm^3/g)	$\sigma(V)$ (cm^3/g)	U (kJ/g)	$\sigma(U)$ (kJ/g)	E (kJ/g)	ΔE_c (kJ/g)	ΔT (K)	ΔE (kJ/g)	ΔV (cm^3/g)
4.84	615	0.7126	0.0090	0.714	0.029	1.174	0.070	−31	−0.045	−0.0102
7.48	1 200	0.6678	0.0059	1.107	0.060	2.062	0.121	−75	−0.115	−0.0015
8.00	1 172	0.6590	0.0074	1.178	0.052	2.107	−0.012	9	0.010	0.0006
9.22	1 606	0.6535	0.0068	1.431	0.052	2.762	0.276	−224	−0.236	−0.0085
10.00	1 557	0.6299	0.0080	1.590	0.061	2.875	0.050	−39	−0.041	−0.0017
11.94	2 206	0.6195	0.0054	1.819	0.056	3.733	0.273	−210	−0.236	−0.0061
12.00	1 957	0.6112	0.0070	1.873	0.071	3.543	0.015	−13	−0.014	−0.0003
12.52	2 355	0.6228	0.0088	1.843	0.059	3.904	0.291	−207	−0.220	−0.0114
15.00	2 585	0.5863	0.0068	2.337	0.091	4.628	0.001	−1	−0.001	0.0000
16.60	3 270	0.5874	0.0092	2.594	0.094	5.575	0.451	−350	−0.348	−0.0123
16.79	3 267	0.5872	0.0074	2.530	0.079	5.508	0.322	−253	−0.285	−0.0044
16.93	3 417	0.5760	0.0060	2.737	0.097	5.867	0.543	−464	−0.536	−0.0008
17.58	3 361	0.5686	0.0054	2.823	0.148	5.896	0.297	−200	−0.296	−0.0001
19.58	3 854	0.5682	0.0079	3.096	0.153	6.671	0.417	−310	−0.357	−0.0061
19.63	3 886	0.5594	0.0066	3.074	0.074	6.681	0.325	−250	−0.282	−0.0044
19.98	4 079	0.5508	0.0103	3.053	0.088	6.858	0.299	−158	−0.218	−0.0081
20.00	3 704	0.5514	0.0070	3.137	0.097	6.559	0.001	0	−0.001	0.0000
20.75	4 362	0.5544	0.0063	3.307	0.106	7.401	0.623	−425	−0.544	−0.0076
21.27	4 308	0.5583	0.0070	3.172	0.105	7.211	0.302	−229	−0.266	−0.0033
21.29	4 765	0.5599	0.0064	3.449	0.104	7.957	1.058	−769	−0.940	−0.0111
22.01	4 769	0.5482	0.0102	3.439	0.121	7.951	0.686	−549	−0.532	−0.0139
23.06	5 156	0.5404	0.0087	3.722	0.178	8.631	0.924	−728	−0.852	−0.0062
25.00	4 915	0.5286	0.0093	3.935	0.245	8.597	0.083	−61	−0.079	−0.0003
30.00	6 218	0.5123	0.0044	4.426	0.108	10.429	−0.056	49	0.054	0.0002
34.90	8 308	0.5054	0.0054	5.319	0.183	13.483	1.144	−951	−1.089	−0.0031
35.00	7 612	0.4999	0.0079	5.194	0.156	12.638	0.166	−141	−0.144	−0.0013
40.00	9 096	0.4775	0.0079	6.179	0.533	15.158	0.441	−290	−0.466	0.0012
45.00	10 675	0.4752	0.0032	6.387	0.132	17.002	0.377	−324	−0.356	−0.0009

($P_0 \approx 0$) yield for specific volume (V_H), density ($\rho_H = 1/V_H$), pressure (P_H), and specific internal energy (E_H) behind the shock front[36]

$$P_H = \rho_0 u_s u_p, \tag{29}$$

$$\rho_H = \rho_0 \left(\frac{u_s}{u_s - u_p} \right), \tag{30}$$

$$E_H = E_0 + \frac{1}{2} P_H (V_0 - V_H) = E_0 + \frac{1}{2} P_H \left(\frac{\rho_H - \rho_0}{\rho_H \rho_0} \right), \tag{31}$$

where u_s is the shock front velocity, u_p is the particle velocity (equal to the piston velocity), and final values have been designated by a subscripted H for Hugoniot. These expressions are known collectively as the Rankine–Hugoniot relations or jump conditions. Equations (29)–(31) identify the locus of states thermodynamically accessible to the sample upon shock compression of a given initial state, and in this they embed considerable information regarding the material equation of state (EOS).

Two important variables in Eq. (31) are E, the specific internal energy or energy per unit mass, and V, specific volume or volume per unit mass. Thermodynamic contributions and simulation averages are discussed most naturally in terms of total energy and volume of an N-particle system or even energy and volume per particle; in order to maximize transparency, we will employ the same variable notation in all these cases. That is, E will designate specific internal energy as well as energy per particle and energy of an N-particle system. Likewise, V will designate related volume variables. It is straightforward to distinguish among usages by context or units. Note that the conversion factor M/N_A is g/particle where M is the molecular weight ($M = 28.0134$ g/mol for N_2) and N_A is Avogadro's number ($6.0221\,367 \times 10^{23}$ particles/mol). Multiplying both sides of Eq. (31) by M/N_A changes the E and V variables from energy/g and volume/g to energy/particle and volume/particle, leaving the equation unchanged except for the meaning of E and V.

E readily separates into three distinct components for a N-particle system,

$$E = E_{\mathrm{id}} + E_v + E_{\mathrm{ex}}, \tag{32}$$

the first two of which can be evaluated using standard forms[37]

$$E_{\mathrm{id}} = \tfrac{5}{2} N k_B T \tag{33}$$

is the ideal translational and rotational contribution of a linear rigid rotor, and

$$E_v = \frac{N k_B \Theta_v}{e^{\Theta_v/T} - 1} \tag{34}$$

is the energy of a quantum harmonic oscillator. The temperature range sampled was too low for electronic excitation to

Downloaded 05 Apr 2010 to 128.206.89.92. Redistribution subject to AIP license or copyright; see http://jcp.aip.org/jcp/copyright.jsp

play a significant role,[38] and the vibrational temperature $\Theta_v = \hbar\omega/k_B$ was evaluated using the experimentally determined nitrogen frequency at zero pressure.[39] Vibrational zero point energy was included separately in the reference heat of formation and specific internal energy E_0, which were determined from measured thermodynamic properties of liquid N_2. The zero of energy is that for isolated N_2 molecules at $T=0$ K. The excess contribution E_{ex} is defined by

$$E_{ex} = \langle U \rangle, \tag{35}$$

where $\langle U \rangle$ is the average configurational energy calculated from *o*-n(MC)^2 simulation.

According to Eq. (31), E_H corresponds to values of E which are zeros of the function

$$f(E) = E - E_0 - \tfrac{1}{2}P(V_0 - V_H), \tag{36}$$

where V_H is chosen as an independent variable, $P(V_H,E)$ is determined by the EOS, and $E_H(V_H)$ is the dependent variable expressed as a function of V_H. Solutions to Eq. (36) define a locus of pressure and temperature combinations $(P=P_H,\ T=T_H)$ comprising the Hugoniot. Maximization of $\overline{A}_{rw}$ with Eq. (28) generated a set of $(P=P_{opt},\ T=T_{opt})$ at which *o*-n(MC)^2 simulations were performed; this set differed from the original, desired $(P=P',\ T=T')$. The original combinations were chosen on the basis of previously reported reweighting calculations,[40,41] as states near the Hugoniot locus. In order to extract thermodynamic information at Hugoniot states from *o*-n(MC)^2 results collected at (P,T) pairs not on the Hugoniot, a mapping between the two sets of conditions must be provided. For (P,T) sufficiently close to (P_H,T_H), volume and energy can be expanded to first order about their simulation values,

$$\begin{aligned} V_H - V \equiv \Delta V \approx & \left.\frac{\partial V}{\partial T}\right|_P (T_H - T) + \left.\frac{\partial V}{\partial P}\right|_T (P_H - P) \\ = & \left.\frac{\partial V}{\partial T}\right|_P \cdot \Delta T + \left.\frac{\partial V}{\partial P}\right|_T \cdot \Delta P, \end{aligned} \tag{37}$$

$$\begin{aligned} E_H - E \equiv \Delta E \approx & \left.\frac{\partial E}{\partial T}\right|_P (T_H - T) + \left.\frac{\partial E}{\partial P}\right|_T (P_H - P) \\ = & \left.\frac{\partial E}{\partial T}\right|_P \cdot \Delta T + \left.\frac{\partial E}{\partial P}\right|_T \cdot \Delta P. \end{aligned} \tag{38}$$

Here, P and T are fixed parameters in the NPT ensemble, while U and V represent the average energy and volume $(U=\langle U\rangle_{P,T},\ V=\langle V\rangle_{P,T})$ calculated from *o*-n(MC)^2 simulation at a prescribed pressure and temperature; E is related to $\langle U \rangle$ by Eqs. (32)–(35). If $P=P_H$ by construction, the second of the two terms in each of the above expansions vanishes; the goal then is to recover the Hugoniot temperature T_H corresponding to a given P_H. Toward this end, Eq. (31) can be restated in terms of differences between simulation results and Hugoniot values,

$$E + \Delta E = E_0 + \tfrac{1}{2}P_H(V_0 - V - \Delta V), \tag{39}$$

into which substitution of Eqs. (37) and (38) produces

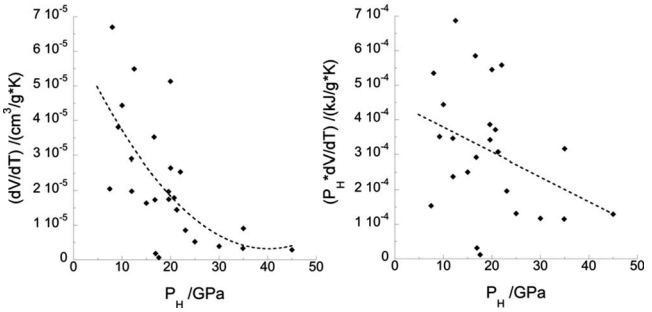

FIG. 4. Partial derivatives of volume with respect to temperature at fixed pressure (left panel), as calculated from results of *o*-n(MC)^2 simulation performed at the $(P=P_{opt},\ T=T_{opt})$ combinations shown in Table IV. The right panel shows the same data, but following multiplication by pressure; as described in the text, these pressures are taken to correspond to Hugoniot values $(P=P_H)$ by construction. The partial derivative is evaluated using Eq. (44), and the dashed lines represent quadratic (left) and linear (right) fits to the data. Note the difference in ordinate scales.

$$E + \left.\frac{\partial E}{\partial T}\right|_P \cdot \Delta T = E_0 + \frac{1}{2}P_H\left(V_0 - V - \left.\frac{\partial V}{\partial T}\right|_P \cdot \Delta T\right). \tag{40}$$

Using Eq. (31) to define the difference between the computed energy E and E_H, then substituting in Eq. (40) gives

$$\begin{aligned} \Delta E_c \equiv & E - E_0 - \frac{1}{2}P_H(V_0 - V) \\ = & -\left(\frac{1}{2}P_H \left.\frac{\partial V}{\partial T}\right|_P + \left.\frac{\partial E}{\partial T}\right|_P\right)\Delta T, \end{aligned} \tag{41}$$

which yields upon slight rearrangement

$$\Delta T = \frac{-\Delta E_c}{\left(\left.\frac{\partial E}{\partial T}\right|_P + \frac{1}{2}P_H \left.\frac{\partial V}{\partial T}\right|_P\right)}, \tag{42}$$

the desired relation. The ideal and quantum harmonic oscillator contributions to $\partial E/\partial T$ are trivial to evaluate using Eqs. (33) and (34), and the rest of the denominator in Eq. (42) can easily be recast (see Appendix B) in terms of simulation parameters and results

$$\left.\frac{\partial\langle U\rangle}{\partial T}\right|_P = \frac{\beta}{T}[P(\langle UV\rangle - \langle U\rangle\langle V\rangle) + \langle U^2\rangle - \langle U\rangle^2], \tag{43}$$

$$\left.\frac{\partial\langle V\rangle}{\partial T}\right|_P = \frac{\beta}{T}[P(\langle UV\rangle - \langle U\rangle\langle V\rangle) + \langle V^2\rangle - \langle V\rangle^2], \tag{44}$$

where ensemble averages once again have been indicated explicitly. P_H and T_H can now be substituted into Eqs. (37) and (38) to produce E_H and V_H. Upon combination of Eqs. (29) and (30) to generate u_s and u_p, the Hugoniot locus is completely specified.

Figures 4 and 5 illustrate in more detail the manner in which Eq. (42) was used to recover temperature values on the Hugoniot. ΔE_c was evaluated using Eqs. (33)–(35), with $\langle U \rangle$ given by the average DFT energy predicted from

Downloaded 05 Apr 2010 to 128.206.89.92. Redistribution subject to AIP license or copyright; see http://jcp.aip.org/jcp/copyright.jsp

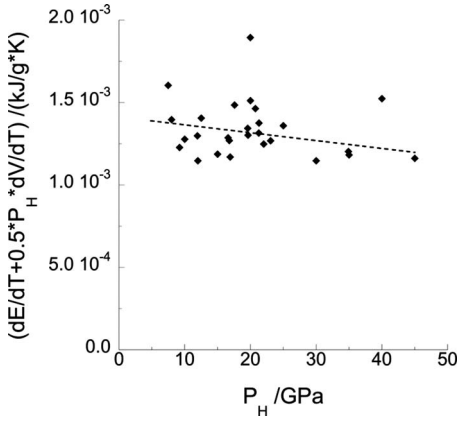

FIG. 5. Evaluation of the denominator appearing in Eq. (42) as calculated from results of o-n(MC)^2 simulation performed at the ($P=P_{\mathrm{opt}}$, $T=T_{\mathrm{opt}}$) combinations shown in Table IV. As described in the text, these pressures are taken to correspond to Hugoniot values ($P=P_H$) by construction and the corresponding Hugoniot values for temperature are recovered by use of Eq. (42). The dashed line is a linear fit to the data.

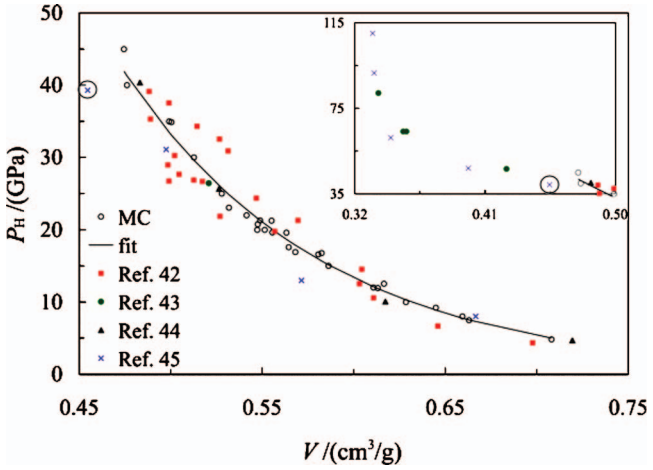

FIG. 6. N_2 Hugoniot in the P-V plane. Experimental results (filled symbols) are taken from Refs. 42–44; theoretical points were calculated using o-N(MC)^2 (open circles, present work) and AIMD (cross, Ref. 45). MC simulations were restricted to the molecular regime (up to $P=40-45$ GPa), and have been shifted according to Eq. (42). The inset displays the high-pressure region that includes ionization; an AIMD result in the transition region has been circled in both the inset and main figure in order to facilitate visual passage between the two. The solid line is an exponential fit through the 28 o-N(MC)^2 data points.

o-n(MC)^2 simulation at the pressure and temperature combinations shown in Table III. The pressures at which simulations were performed were also taken to fall on the Hugoniot (*vide supra*), and the derivatives appearing in the denominator of Eq. (42) were evaluated using Eqs. (43) and (44) and the equilibrium averages computed from simulation. The derivative of volume with respect to temperature at each ($P=P_{\mathrm{opt}}\equiv P_H$, $T=T_{\mathrm{opt}}$) combination is shown in Fig. 4 (left panel), as well these derivatives multiplied by their corresponding pressures (right panel). The data in the left and right panels are fit to linear and quadratic functions (dashed lines), respectively. Figure 5 illustrates the entire denominator of Eq. (42) built from the component pieces appearing in Fig. 4.

Recovery of T_H permitted determination of V_H through application of Eq. (37), enabling construction of the N_2 Hugoniot locus in Fig. 6 (P-V plane) and Fig. 7 (u_s-u_p plane). The nitrogen Hugoniot has been measured[42–44] or calculated[38,40,41] on a number of occasions previously, but only in a few instances have calculations using a self-consistent potential such as DFT[40,45,46] been reported. Open circles in Fig. 6 represent o-n(MC)^2 results calculated at ($P_{\mathrm{opt}}, T_{\mathrm{opt}}$) and then shifted to the Hugoniot locus (P_H, T_H) in the manner described above. The solid line is a fit of those results to an exponential function. Although components of the shifts (illustrated in Figs. 4 and 5) possess relatively large uncertainties, the net uncertainties are comparable to or smaller than the statistical uncertainties in the simulated states themselves; error estimates are given in Table IV but omitted from the figures for clarity. The 28 MC data points shown explicitly in Fig. 6 have been replaced with a quadratic fit in Fig. 7 for ease of viewing, but otherwise symbols and shading have been preserved across the two figures for each data set depicted. Agreement with experimental data in the molecular regime—which we take to be 40–45 GPa or less—taken from Refs. 42 (squares), 43 (filled circles), and 44 (triangles) is excellent. [See the following paragraph for discussion of the higher pressure region for which the o-n(MC)^2 methodology was not applied.] In addition to the experimental results we have included those of a previous calculation[45] made using *ab initio* molecular dynamics (AIMD) in the *NVT* ensemble with a PW91 exchange-correlation functional and Vanderbilt ultrasoft pseudopotentials[47] (crosses). This particular implementation was designed specifically to capture electronic and dissociation effects in the high temperature and pressure region; however, the small system size (32 atoms=16 molecules) and the use of pseudopotentials introduce uncertainties that are difficult to quantify. Only four of the calculated points fell in the molecular regime, but these were in qualitative agreement with experiment. The shock and particle veloci-

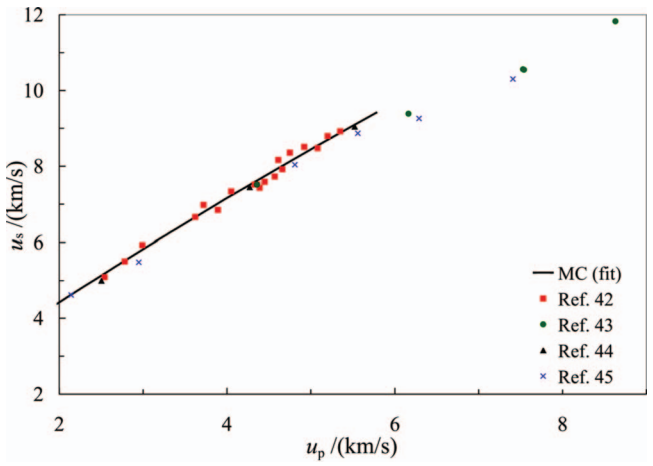

FIG. 7. N_2 Hugoniot in the u_s-u_p plane. Experimental results (filled symbols) are taken from Refs. 42–44; theoretical results were calculated using o-N(MC)^2 (solid line, present work) and AIMD (cross Ref. 45). MC simulations were restricted to the molecular regime (up to $P=40-45$ GPa), and have been shifted according to Eq. (42). Here, for ease of viewing, the 28 individual o-N(MC)^2 points results shown explicitly in Fig. 6 were replaced by a quadratic fit after transformation between the P-V and u_s-u_p planes.

Downloaded 05 Apr 2010 to 128.206.89.92. Redistribution subject to AIP license or copyright; see http://jcp.aip.org/jcp/copyright.jsp

ties, u_s and u_p, in Fig. 7 are based on the same fundamental information as are P and V in Fig. 6 (P_H and V_H are derived from u_s, u_p, and the Hugoniot jump conditions, Eqs. (29)–(31), although the relationship in the u_s-u_p plane is nearly linear. Again, however, the trend is that the present calculations are in excellent agreement with the experimental data below $u_p \approx 6$ km/s.

Thus far we have focused exclusively on pressures of 45 GPa and below, but Figs. 6 and 7 also include higher pressure regions where dissociation, ionization, and electronically excited states become important. Trends in the experimental data of Nellis *et al.*[43] and AIMD simulation results of Kress *et al.*[45] are in good agreement generally, and both clearly reflect an abrupt change between $P=40$ and 47 GPa; here we focus specifically on the transition region in which dissociation emerges as an important factor. At $P=31$ GPa, the specific volume predicted by *ab initio* molecular dynamics AIMD (with $7\pm3\%$ dissociation) is near the average of the measured data scatter (Fig. 6); at 39 GPa ($16\pm9\%$ dissociation by interpolation of Table I in Ref. 45) it is significantly less than that predicted by experiment. These facts suggest that the calculated dissociation is overestimated in the transition region. By way of contrast, the present results fall well within the experimental scatter for pressures up to 40 GPa. If dissociation were important in this region, we would expect the o-N(MC)^2 results to begin to deviate from experiment at pressures lower than those for which they actually do. Taken collectively, the measured and calculated data suggest that dissociation is not significant to the Hugoniot below the transition region found at $P\sim40-45$ GPa. This transition region *could* reflect to a two-wave structure, in which case shock velocity u_s is established by a leading wave whereas the particle velocity u_p is determined on the basis of either thermodynamics or kinetics that leads to a secondary wave propagating in the material. Examples where this could occur include a first order phase transition with a large volume change or relaxation from the highest metastable state that can be maintained before the kinetics allow a return to equilibrium on a time scale that is short compared to the time resolution of the shock experiment. If a single wave is assumed in such an instance, then the predicted P and V will be incorrect. The hallmark of two-wave structure is constant u_s across some interval of u_p; but, unfortunately, there is only one data point in the transition region shown. For this reason, it is unclear whether the data reflect a *bona fide* two-wave structure or merely a region of rapid transition.

Note that the present calculations assume the validity of the rigid rotor and quantum harmonic oscillator approximations. Raman line shifts in liquid nitrogen singly shocked to $P=10-20$ GPa and doubly shocked to $P=15-40$ GPa have been measured[48] and calculated using a first-principles approach.[49] Both fundamental ($0\rightarrow1$) and hot band ($1\rightarrow2$, $2\rightarrow3$, and $3\rightarrow4$) transitions indicated that vibrational energies increased $\sim1\%$ in the singly shocked state and $\sim2\%$ in the doubly shocked state. There was no indication of vibrational potential softening even at the highest pressure measured; the data imply rather that vibrations are very weakly coupled to other modes, in conformity with the assumptions made here. We have treated shocked nitrogen in the molecular phase as undergoing negligible electronic excitation as well, given that the lowest electronic excited state in N_2 has a relative energy of roughly 6 eV. This energy, and the ground state dissociation energy of approximately 10 eV, are to be compared with a temperature equivalent of 1 eV or less on the principal Hugoniot up to $P\sim45$ GPa.

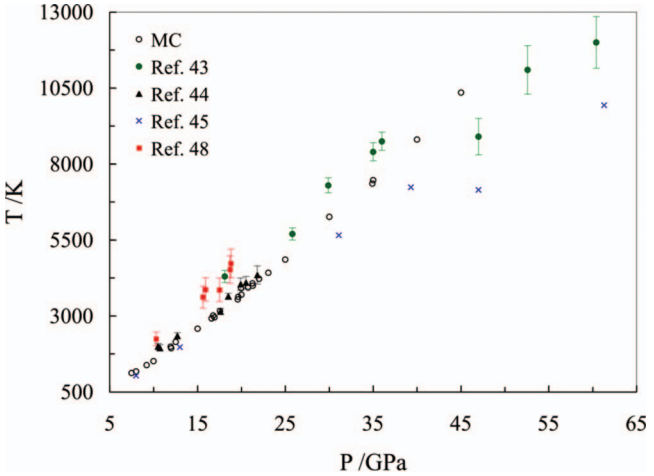

FIG. 8. Temperatures measured (filled symbols, Refs. 43, 44, and 48) or calculated (Ref. 45 and present work) on the N_2 Hugoniot.

Several techniques for temperature measurement on the Hugoniot have been reported previously, each of which potentially introduces systematic errors of unknown magnitude due to assumptions made in the analysis. Figure 8 shows measured data compared with the present calculations and those of Kress *et al.*[45] The temperature data of Nellis *et al.*[43] increase along a trend line that coincides well with the MC results up to $P=36$ GPa, as would be expected under conditions of negligible dissociation. The next highest temperature measurement, obtained at $P=47$ GPa is significantly cooler than this trend predicts, as would be expected should onset of significant dissociation occur for conditions between the two measured data points. A new trend is established at higher pressure, corresponding to a partially dissociated phase in which some fraction of kinetic energy has been expended to break the nitrogen triple bond, resulting in lower temperatures than would be found for molecular nitrogen. The interpretation of the temperature data is the same as that of the P-V and u_s-u_p results: There is negligible dissociation at pressures below 40–45 GPa, but a significant amount at pressures higher than this.

V. SUMMARY AND CONCLUSIONS

We have used the o-n(MC)^2 algorithm with a DFT potential to generate the Hugoniot locus of N_2 fluid for pressures and temperatures relevant to HE detonation. After collecting several hundred configurations at which to evaluate δW for a number of (P,T) combinations, the *a priori* acceptance probability defined by Eq. (27) was maximized as a function of P and T to yield optimal thermodynamic conditions at which to perform n(MC)^2 sampling. The o-n(MC)^2 simulations were then carried out at temperature and pressure combinations not necessarily on the Hugoniot locus, but

Downloaded 05 Apr 2010 to 128.206.89.92. Redistribution subject to AIP license or copyright; see http://jcp.aip.org/jcp/copyright.jsp

from which Hugoniot states could be recovered by use of the expansion procedure defined in Eqs. (37) and (38) and culminating in Eqs. (42)–(44). The method yields both high accuracy and high precision. It is worth noting that in contrast to previous calculations[45] the current approach includes all electrons (no pseudopotential approximation) and readily accommodates a system more than six times larger than the earlier study, thereby reducing the likelihood of finite-size effects in the results.

An analytical reference potential was used in this work, but *o*-n$(MC)^2$ should work equally well with two different *ab initio*, DFT, or semiempirical potentials. The reference potential could rely on a more approximate algorithm or a smaller basis set, so long as (1) its correspondence to the full potential still permits a reasonable offset O between full energy evaluations and (2) it can still be evaluated rapidly. The full potential would then consist of a fully converged calculation at a higher level of theory.

The *o*-n$(MC)^2$ method provides a versatile framework in which to carry out precision MC sampling of accurate potentials, and it would be worthwhile to make detailed comparison of its performance to that of AIMD.[50] Straightforward formulation of efficiency metrics such as Eq. (24) is impossible without determination of a quantitative relation between the average single-particle displacement in accepted MC steps and in AIMD time steps. This is a nontrivial task, and perhaps it would be simpler to calculate the number of AIMD steps required to yield decorrelated configurations, then compare this with the number of composite *o*-n$(MC)^2$ steps needed for the same purpose; even given these two quantities, still it is not at all clear that their ratio would not vary strongly from one system to the next. Aside from efficiency considerations, MC methods accommodate generalized ensemble sampling much more naturally than does MD, some of the advantages of which (e.g., the ability to calculate transport properties) disappear when standard thermostats and barostats are invoked due to their inherently stochastic foundation.[51]

ACKNOWLEDGMENTS

J.D.C. thanks the Office of the Director at Los Alamos National Laboratory (LANL) for the support in the form of a Director's Postdoctoral Fellowship. M.S.S. is supported by the LANL High Explosives Project of the National Nuclear Security Administration (NNSA) Advanced Strategic Computing Program (HE-ASC). T.D.S. is supported by the LANL Laboratory Directed Research and Development (LDRD) Program and by the (U.S.) Army Research Office under Grant No. W911NF-05-1-0265. LANL is operated by Los Alamos National Security L.L.C. under the auspices of the NNSA and the United States Department of Energy under Contract No. DE-AC52-06NA25396.

APPENDIX A: AVERAGE MANY-BODY CONTRIBUTION PER PAIR

Here we prove the claim that $U_{AB}^{*}-U_{AB}^{(2)}$ as defined by Eqs. (13) and (14) in the text gives an average many-body contribution per pair that, when summed over all A and B, returns the total configurational energy of the system under the assumption that many-body effects terminate at third order. The total energy as a sum of two- and three-body interactions is given by

$$U_{\mathrm{box}}=\frac{1}{2}\sum_{\substack{i=1\\ i\neq j}}^{N}\sum_{j=1}^{N}\varphi_{ij}+\frac{1}{6}\sum_{\substack{i=1\\ i\neq j\neq k}}^{N}\sum_{j=1}^{N}\sum_{k=1}^{N}\lambda_{ijk}=U_{N}^{(2)}+U_{N}^{(3)}, \tag{A1}$$

where $U_{x}^{(y)}$ represents the y-body contribution to the total energy of a x-particle system. Let $U_{\text{box-}A}$ equal the box energy with molecule A removed,

$$\begin{aligned}U_{\text{box-}A}&=\frac{1}{2}\sum_{\substack{i=1\\ i\neq j\neq A}}^{N}\sum_{j=1}^{N}\varphi_{ij}+\frac{1}{6}\sum_{\substack{i=1\\ i\neq j\neq k=A}}^{N}\sum_{j=1}^{N}\sum_{k=1}^{N}\lambda_{ijk}=U_{\mathrm{box}}-\frac{1}{2}\sum_{\substack{j=1\\ j\neq A}}^{N}\varphi_{Aj}\\&\quad-\frac{1}{2}\sum_{\substack{i=1\\ i\neq A}}^{N}\varphi_{iA}-\frac{1}{6}\sum_{\substack{j=1\\ j\neq k\neq A}}^{N}\sum_{k=1}^{N}\lambda_{Ajk}-\frac{1}{6}\sum_{\substack{i=1\\ i\neq k\neq A}}^{N}\sum_{k=1}^{N}\lambda_{iAk}\\&\quad-\frac{1}{6}\sum_{\substack{i=1\\ i\neq j\neq A}}^{N}\sum_{j=1}^{N}\lambda_{ijA}=U_{\mathrm{box}}-\sum_{j=1}^{N}\varphi_{Aj}-\frac{1}{2}\sum_{\substack{i=1\\ i\neq j\neq A}}^{N}\sum_{j=1}^{N}\lambda_{ijA},\end{aligned} \tag{A2}$$

and assume an analogous relation for $U_{\text{box-}B}$. When both A and B are removed together,

$$\begin{aligned}U_{\text{box-}AB}&=\frac{1}{2}\sum_{\substack{i=1\\ i\neq j\neq A\neq B}}^{N}\sum_{j=1}^{N}\varphi_{ij}+\frac{1}{6}\sum_{\substack{i=1\\ i\neq j\neq k\neq A}}^{N}\sum_{j=1}^{N}\sum_{k=1}^{N}\lambda_{ijk}=U_{\mathrm{box}}-\frac{1}{2}\sum_{\substack{j=1\\ j\neq A}}^{N}\varphi_{Aj}-\frac{1}{2}\sum_{\substack{i=1\\ i\neq A}}^{N}\varphi_{iA}-\frac{1}{6}\sum_{\substack{j=1\\ j\neq k\neq A}}^{N}\sum_{k=1}^{N}\lambda_{Ajk}-\frac{1}{6}\sum_{\substack{i=1\\ i\neq k\neq A}}^{N}\sum_{k=1}^{N}\lambda_{iAk}-\frac{1}{6}\sum_{\substack{i=1\\ i\neq j\neq A}}^{N}\sum_{j=1}^{N}\lambda_{ijA}\\&=U_{\mathrm{box}}-\sum_{j=1}^{N}\varphi_{Aj}-\frac{1}{2}\sum_{\substack{i=1\\ i\neq j\neq A}}^{N}\sum_{j=1}^{N}\lambda_{ijA}-\frac{1}{2}\sum_{\substack{i=1\\ i\neq j\neq B}}^{N}\sum_{k=1}^{N}\lambda_{ijB}+\frac{1}{2}(\varphi_{AB}+\varphi_{AB})+\frac{1}{6}\sum_{\substack{k=1\\ k\neq A,B}}^{N}(\lambda_{ABk}+\lambda_{AkB}+\lambda_{kAB}+\lambda_{BAk}+\lambda_{BkA}+\lambda_{kBA})\\&=E+(E_{\text{box-}A}-E_{\mathrm{box}})+(E_{\text{box-}B}-E_{\mathrm{box}})+\varphi_{AB}+\sum_{\substack{k=1\\ k\neq A,B}}^{N}\lambda_{ABk}.\end{aligned} \tag{A3}$$

Downloaded 05 Apr 2010 to 128.206.89.92. Redistribution subject to AIP license or copyright; see http://jcp.aip.org/jcp/copyright.jsp

From Eq. (A3) one can define an effective pair energy including an average many-body correction as

$$U_{AB}^{*} \equiv \varphi_{AB} + \sum_{\substack{k=1 \\ k\neq A,B}}^{N} \lambda_{ABk} = U_{\text{box}} + U_{\text{box-}AB} - U_{\text{box-}A} - U_{\text{box-}B}, \tag{A4}$$

equivalent to Eq. (14) in the text. Note that

$$\frac{1}{2}\sum_{\substack{i=1 \\ i\neq j}}^{N}\sum_{j=1}^{N} U_{ij}^{*} = \frac{1}{2}\sum_{\substack{i=1 \\ i\neq j}}^{N}\sum_{j=1}^{N} \varphi_{ij} + \frac{1}{2}\sum_{\substack{i=1 \\ i\neq j\neq k}}^{N}\sum_{j=1}^{N}\sum_{k=1}^{N} \lambda_{ijk} = U_N^{(2)} + 3U_N^{(3)} \tag{A5}$$

by comparison with Eq. (A1). If the difference between effective pair and standard pair energies is defined as $\delta U_{ij} \equiv U_{ij}^{*} - U_{ij}^{(2)}$, then the average value of these three quantities in a N-body system is given by

$$\overline{U^{*}} = \frac{1}{N(N-1)}\sum_{\substack{i=1 \\ i\neq j}}^{N}\sum_{j=1}^{N} U_{ij}^{*}, \tag{A6}$$

$$\overline{U^{(2)}} = \frac{1}{N(N-1)}\sum_{\substack{i=1 \\ i\neq j}}^{N}\sum_{j=1}^{N} U_{ij}^{(2)}, \tag{A7}$$

$$\overline{\delta U} = \frac{1}{N(N-1)}\sum_{\substack{i=1 \\ i\neq j}}^{N}\sum_{j=1}^{N} \delta U_{ij}, \tag{A8}$$

and the total values by

$$U_N^{*} = \frac{N(N-1)}{2}\overline{U^{*}}, \tag{A9}$$

$$U_N^{(2)} = \frac{N(N-1)}{2}\overline{U^{(2)}}, \tag{A10}$$

$$\delta U_N = \frac{N(N-1)}{2}\overline{\delta U}. \tag{A11}$$

The box energy expressed in terms of Eqs. (A10) and (A11) is then

$$U_{\text{box}} = U_N^{(2)} + \delta U_N. \tag{A12}$$

By equating the box energy of Eq. (A5) with that of Eq. (A12) one finds that

$$3U_N^{(3)} = \frac{1}{2}\sum_{\substack{i=1 \\ i\neq j}}^{N}\sum_{j=1}^{N} \delta U_{ij}, \tag{A13}$$

the relation to be proved.

APPENDIX B: DERIVATION OF EQUATIONS (43) and (44)

Treating $\langle U\rangle$ as a function of $\beta=(kT)^{-1}$ and applying the chain rule,

$$\left.\frac{\partial\langle U\rangle}{\partial T}\right|_P = \frac{\partial\beta}{\partial T}\left.\frac{\partial\langle U\rangle}{\partial\beta}\right|_P. \tag{B1}$$

The first factor is trivial,

$$\frac{\partial\beta}{\partial T} = -\frac{\beta}{T}. \tag{B2}$$

Recall that an ensemble-averaged quantity X is defined as

$$\langle X\rangle \equiv \frac{\int\int X e^{W} d\tau dV}{\int\int e^{W} d\tau dV}, \tag{B3}$$

where W represents the thermodynamic weight appropriate to the ensemble being sampled; for the isothermal-isobaric ensemble, W is given in Eq. (16) of the text. For the sake of brevity we drop the explicit indication of constant P in the derivatives of Eq. (B1) and the $N\ln V$ factor appearing in the exponential of Eq. (16), then write out explicitly the integrals appearing in the right-hand side of Eq. (B1),

$$\frac{\partial\langle U\rangle}{\partial\beta} = -\frac{(\int\int (U+PV)Ue^{-\beta(U+PV)}d\tau dV)(\int\int e^{-\beta(U+PV)}d\tau dV)}{(\int\int e^{-\beta(U+PV)}d\tau dV)^2} + \frac{(\int\int Ue^{-\beta(U+PV)}d\tau dV)(\int\int (U+PV)e^{-\beta(U+PV)}d\tau dV)}{(\int\int e^{-\beta(U+PV)}d\tau dV)^2}. \tag{B4}$$

Using Eq. (B3), Eq. (B4) becomes

$$\frac{\partial\langle U\rangle}{\partial\beta} = -\langle U(U+PV)\rangle + \langle U\rangle\langle U+PV\rangle = P(\langle U\rangle\langle V\rangle - \langle UV\rangle) + \langle U\rangle^2 - \langle U^2\rangle. \tag{B5}$$

Combining Eqs. (B2) and (B5) gives

$$\left.\frac{\partial\langle U\rangle}{\partial T}\right|_P = \frac{\beta}{T}[P(\langle UV\rangle - \langle U\rangle\langle V\rangle) + \langle U^2\rangle - \langle U\rangle^2], \tag{B6}$$

identical to Eq. (43) in the text. The derivation of Eq. (44) proceeds in a fashion perfectly analogous to that detailed here for Eq. (40).

Downloaded 05 Apr 2010 to 128.206.89.92. Redistribution subject to AIP license or copyright; see http://jcp.aip.org/jcp/copyright.jsp

[1] See the Shock Compression of Condensed Matter series in the AIP Conference Proceedings, available at http://proceedings.aip.org/proceedings/top.jsp.
[2] M. J. Gillain, D. Alfe, J. Brodholt, L. Vocadlo, and G. D. Price, Rep. Prog. Phys. **69**, 2365 (2006).
[3] D. J. Depaolo and F. M. Orr, Phys. Today **61**(8), 46 (2008).
[4] *IPCC Special Report on Carbon Dioxide Capture and Storage*, edited by B. Metz (Cambridge University Press, Cambridge, 2004).
[5] M. P. Allen and D. J. Tildesley, *Computer Simulation of Liquids* (Oxford University Press, Oxford, 1987).
[6] D. Frenkel and B. Smit, *Understanding Molecular Simulation: From Algorithms to Applications* (Academic, New York, 2002).
[7] Y. B. Zel'dovitch and Y. P. Raizer, *Physics of Shock Waves and High-Temperature Hydrodynamic Phenomena* (Dover, Mineola, NY, 2002).
[8] J. D. Coe, T. D. Sewell, and M. S. Shaw, J. Chem. Phys. **130**, 164104 (2009).
[9] R. Iftimie, D. Salahub, D. Wei, and J. Schofield, J. Chem. Phys. **113**, 4852 (2000).
[10] L. D. Gelb, J. Chem. Phys. **118**, 7747 (2003).
[11] W. Koch and M. C. Holthausen, *A Chemist's Guide to Density Functional Theory*, 2nd ed. (Wiley-VCH, Weinheim, FRG, 2001); R. G. Parr and W. Yang, *Density-Functional Theory of Atoms and Molecules* (Oxford University Press, New York, 1989).
[12] P. Hohenberg and W. Kohn, Phys. Rev. **136**, B864 (1964).
[13] W. Kohn and L. J. Sham, Phys. Rev. **140**, A1133 (1965).
[14] J. P. Perdew and A. Zunger, Phys. Rev. B **23**, 5048 (1981).
[15] K. Burke, J. P. Perdew, and Y. Wang, in *Electronic Density Functional Theory: Recent Progress and New Directions*, edited by J. F. Dobson, G. Vignale, and M. P. Das (Plenum, New York, 1998).
[16] C. C. J. Roothaan, Rev. Mod. Phys. **23**, 69 (1951).
[17] M. J. Frisch, G. W. Trucks, H. B. Schlegel *et al.*, GAUSSIAN 03, Revision C.02, Gaussian, Inc., Wallingford CT, 2004.
[18] A. D. Becke, Phys. Rev. A **38**, 3098 (1988).
[19] C. Lee, W. Yang, and R. G. Parr, Phys. Rev. B **37**, 785 (1988).
[20] J. P. Perdew, K. Burke, and M. Ernzerhof, Phys. Rev. Lett. **77**, 3865 (1996).
[21] J. P. Perdew, in *Electronic Structure of Solids*, edited by P. Ziesche and H. Eschrig (Akademie Verlag, Berlin, 1991).
[22] S. H. Vosko, L. Wilk, and M. Nusair, Can. J. Phys. **58**, 1200 (1980).
[23] C. Pisani, *Quantum-Mechanical Ab-Initio Calculation of the Properties of Crystalline Materials* (Springer-Verlag, Berlin, 1996).
[24] J. B. Collins, P. R. Schleyer, J. S. Binkley, and J. A. Pople, J. Chem. Phys. **64**, 5142 (1976); W. J. Hehre, R. F. Stewart, and J. A. Pople, *ibid.* **51**, 2657 (1969).
[25] A. D. McLean and G. S. Chandler, J. Chem. Phys. **72**, 5639 (1980).
[26] S. F. Boys and F. Bernardi, Mol. Phys. **19**, 553 (1970).
[27] M. J. Frisch, J. A. Pople, and J. S. Binkley, J. Chem. Phys. **80**, 3265 (1984).
[28] W. J. Hehre, R. Ditchfield, and J. A. Pople, J. Chem. Phys. **56**, 2257 (1972).
[29] C. Moller and M. S. Plesset, Phys. Rev. **46**, 618 (1934).
[30] J. C. Slater, Phys. Rev. **81**, 385 (1951).
[31] A. J. Stone, *The Theory of Intermolecular Forces* (Oxford University Press, Oxford, 1996).
[32] The pair was chosen on the basis of its placement at roughly the center of the simulation cell and its constituents being "nearest neighbors" and thus sharing a substantial repulsive interaction.
[33] N. Metropolis, A. W. Rosenbluth, M. N. Rosenbluth, A. H. Teller, and E. Teller, J. Chem. Phys. **21**, 1087 (1953).
[34] W. W. Wood, in *Physics of Simple Liquids*, edited by J. S. Rowlinson and G. S. Rushbrooke (Wiley, New York, 1968), p. 115.
[35] I. R. McDonald and K. Singer, J. Chem. Phys. **47**, 4766 (1967).
[36] R. Courant and K. O. Friedrichs, *Supersonic Flow and Shock Waves* (Springer, New York, 1999).
[37] See, for instance, D. A. McQuarrie, *Statistical Mechanics* (University Science Books, Sausalito, CA, 2000).
[38] J. D. Johnson, M. S. Shaw, and B. L. Holian, J. Chem. Phys. **80**, 1279 (1983).
[39] G. Herzberg, *Spectra of Diatomic Molecules* (Van Nostrand Reinhold, New York, 1950).
[40] M. S. Shaw and C. Tymczak, in *Shock Compression of Condensed Matter*, edited by M. D. Furnish (American Institute of Physics, Melville, NY, 2005), Vol. 845, p. 179.
[41] M. S. Shaw and C. Tymczak, in *Proceedings of the 13th Internation Detonation Symposium* edited by J. Kennedy (Office of Naval Research, Norfolk, VA, 2006), Paper No. ONR 351-07-01, p. 1181.
[42] R. D. Dick, J. Chem. Phys. **52**, 6021 (1970).
[43] W. J. Nellis, N. C. Holmes, A. C. Mitchell, and M. van Thiel, Phys. Rev. Lett. **53**, 1661 (1984); W. J. Nellis and A. C. Mitchell, J. Chem. Phys. **73**, 6137 (1980); W. J. Nellis, H. B. Radousky, D. C. Hamilton, A. C. Mitchell, N. C. Holmes, K. B. Christianson, and M. van Thiel, *ibid.* **94**, 2244 (1991).
[44] V. N. Zubarev and G. S. Telegin, Sov. Phys. Dokl. **7**, 34 (1962).
[45] J. D. Kress, S. Mazevet, L. A. Collins, and W. W. Wood, Phys. Rev. B **63**, 024203 (2000).
[46] S. Mazevet, J. D. Johnson, J. D. Kress, L. A. Collins, and P. Blottiau, Phys. Rev. B **65**, 014204 (2001).
[47] D. Vanderbilt, Phys. Rev. B **41**, 7892 (1990).
[48] D. S. Moore, S. C. Schmidt, M. S. Shaw, and J. D. Johnson, J. Chem. Phys. **90**, 1368 (1989).
[49] J. D. Coe, T. D. Sewell, M. S. Shaw, and E. M. Kober, Chem. Phys. Lett. **464**, 265 (2008).
[50] R. Car and M. Parrinello, Phys. Rev. Lett. **55**, 2471 (1985); M. E. Tuckerman, J. Phys.: Condens. Matter **14**, R1297 (2002).
[51] P. H. Hunenberger, Adv. Polym. Sci. **173**, 105 (2005).
[52] R. Ditchfield, W. J. Hehre, and J. A. Pople, J. Chem. Phys. **54**, 724 (1971).
[53] R. Krishnan, J. S. Binkley, R. Seeger, and J. A. Pople, J. Chem. Phys. **72**, 650 (1980).

Downloaded 05 Apr 2010 to 128.206.89.92. Redistribution subject to AIP license or copyright; see http://jcp.aip.org/jcp/copyright.jsp